

# Predictive Coding Based Multiscale Network with Encoder-Decoder LSTM for Video Prediction

Chaofan Ling<sup>1</sup>, Junpei Zhong<sup>† 2</sup>, and Weihua Li<sup>† 1</sup>

<sup>1</sup>South China University of Technology, Guangzhou, China

<sup>2</sup>The Hong Kong Polytechnic University, KLN, Hong Kong

**Abstract**—We are introducing a multi-scale predictive model for video prediction here, whose design is inspired by the “Predictive Coding” theories and “Coarse to Fine” approach. As a predictive coding model, it is updated by a combination of bottom-up and top-down information flows, which is different from traditional bottom-up training style. Its advantage is to reduce the dependence on input information and improve its ability to predict and generate images. Importantly, we achieve with a multi-scale approach—higher level neurons generate coarser predictions (lower resolution), while the lower level generate finer predictions (higher resolution). This is different from the traditional predictive coding framework in which higher level predict the activity of neurons in lower level. To improve the predictive ability, we integrate an encoder-decoder network in the LSTM architecture and share the final encoded high-level semantic information between different levels. Additionally, since the output of each network level is an RGB image, a smaller LSTM hidden state can be used to retain and update the only necessary hidden information, avoiding being mapped to an overly discrete and complex space. In this way, we can reduce the difficulty of prediction and the computational overhead. Finally, we further explore the training strategies, to address the instability in adversarial training and mismatch between training and testing in long-term prediction. Code is available at <https://github.com/Ling-CF/MSPN>

**Index Terms**—Predictive coding, video frame prediction, adversarial training.

## I. INTRODUCTION

The ability to predict the future has recently received increased attention. The idea that human brain is essentially a “prediction machine” is one of the accepted theories in the field of cognitive science. According to the famous “predictive coding” theory, various functions of the brain, including perception, memory, behavior control, etc., are shaped and realized through prediction [1]–[4], which shows the importance of predictive ability. Actually, prediction based on context information is also essential in the field of machine learning, among which future video frame prediction is a research that has developed rapidly in recent years [5]–[8].

It is a pixel-intensive prediction task that predicts and generates future frames by learning historical video information (Fig 1). This looking-ahead ability can be applied to various fields such as autonomous driving [9], [10], robot navigation [11], precipitation prediction [12], pedestrian trajectory prediction [13], activities and events prediction [14]. Specifically, the

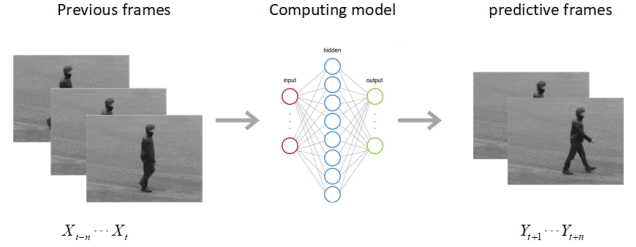


Fig. 1. Computational model learns to predict future frames ( $Y_{t+1}, \dots, Y_{t+m}$ ) by analyzing spatial-temporal relationships in the previous video frames ( $X_{t-n}, \dots, X_t$ )

predictive ability provides a variety of possibilities for the learning system: it endows the self-driving car to forecast changes in the traffic situation to make actions beforehand. Mobile robots can also better plan paths by predicting the moving direction and speed for dynamic obstacles. In particular, this special self-supervised learning of video representations can also be transferred to downstream tasks [15], [16]—self-supervised video prediction learning is first performed on the backbone network, and then its parameters are fixed and used for tasks such as video classification, thereby alleviating the difficulty of label acquisition in supervised learning tasks.

However, predicting how future scenarios will unfold is a challenging work. Firstly, real-world events are diverse and stochastic, which poses great challenges for deterministic prediction. Secondly, the curse of dimensionality makes it more difficult to predict an accurate and sharp image. The existing models or methods still suffer from lack of appearance details and low prediction accuracy. These problems become increasingly severe as prediction errors accumulate over time during long-term prediction. In addition, the huge computational overhead is also a major problem that plagues video prediction. For example, E3D-LSTM additionally embeds the complex 3D convolution calculations into the LSTM network [17] in an attempt to better capture short-term information, but this results in exponential increases in computational overhead—each of their predictions needs to be computed with several input frames. In order to solve the above problems, this paper proposes a method that combines the theoretical framework of predictive coding and “coarse to fine” approach to design a more efficient network model.

In the field of cognitive science, predictive coding is one of the most important cognitive frameworks. It argues that

Corresponding author: Junpei Zhong, [joni.zhong@polyu.edu.hk](mailto:joni.zhong@polyu.edu.hk)  
Corresponding author: Weihua Li, [whlee@scut.edu.cn](mailto:whlee@scut.edu.cn)

there is an internal model in the brain that continuously generates and updates a representation of the environment, which is used to generate predictions that are compared with actual sensory inputs, to generate prediction errors. These prediction errors are then used to update and correct the intrinsic representation model. Hierarchical processing is the central idea of the predictive coding framework, with the lowest level neurons receiving sensory input from the outside world and passing prediction errors upward, and higher level processing prediction errors from lower level and generate predictions for downward propagation. The entire model is updated through a combination of bottom-up and top-down information flows, so it does not rely solely on external information. Furthermore, the propagation of prediction errors also constitutes an efficient feedback connection, which is another advantage of the predictive coding model. The specific calculation framework can refer to [1].

We construct a multi-scale predictive network (MSPN) based on the above computational framework. But different from the traditional computational style of predictive coding, each level of our network predicts an RGB image, rather than the activity of neurons in lower level. This idea is inspired by the coarse-to-fine approach. We implement the computation with a multi-layer convolutional LSTM architecture. The input of each level is simple, only including the RGB predicted image from higher level, the prediction errors of current level and lower level. Since they are pixel-level inputs, it is necessary to use an encoder-decoder network to implement the extraction of high-level semantic features and the generation of images. It may increase the computational overhead and the number of parameters, but we indicate that for the smaller-resolution inputs of higher-level, fewer network layers and parameters is enough. And since we generate RGB images in each level, the hidden state of LSTM can be fixed to a smaller depth (such as  $c = 64$ , where  $c$  denotes the channels), only retaining and updating the information necessary to generate RGB images. This not only reduces computational overhead, but also prevents the hidden state from being mapped to a more discrete and complex space, thus reducing the difficulty of prediction. In addition, in order to enhance the connection between different levels, we share the encoded highest-level semantic information, which will be introduced in detail in Section 3.

In addition to the network architecture, the training strategy is also important. We use adversarial training to sharpen generated images and propose a solution to the problem of adversarial training instability. Specifically, the discriminator is ensured to be always slightly stronger than the generator, which can prevent the discriminator from overtraining and the generator from learning the wrong gradient. Aiming at the problem of mismatch between training and testing in sequence tasks, we also propose corresponding improvement methods. The detail will be also introduced in Section 3.

The rest of this paper is organized as follows: First, Section 2 briefly reviews the related works about video prediction from the perspective of network architecture, training manner and so on. Next, Section 3 introduces the structure of network model and training methods in detail. Then, Section 4 demonstrates

the experiments including experimental setting, quantitative results and qualitative results. Finally, Section 5 summarizes the paper and draws conclusions about this work.

## II. RELATED WORK

Building on the great success of deep learning, research on video prediction has received more and more attention. Early works focused on directly predicting pixel intensities by implicitly modeling scene dynamics and underlying information. To simplify the prediction task, some people try to decompose the video into motion and content, process them on separate paths, to decompose the prediction task into a more tractable problem. Subsequently, generative adversarial training has shown encouraging performance on image generation, and adversarial training-based stochastic video prediction methods have also exploded. In addition, methods based on 3D convolution and predictive coding are also worthy of attention. Next, we will briefly classify and summarize the above video prediction methods, and introduce some of the most representative models and methods.

The MCNet [18] first proposed the separation of motion and content. The authors encode the local dynamics and spatial layout separately, in which they only predict the motion state, and finally fuse with the content to obtain the predicted frame. However, the referred motion is obtained by subtracting the previous frame from the subsequent frame, which only describes the changes at the pixel level. So when the scene is complex and varied, it is disastrous. In order to better learn the motion information of objects, Chen et al. proposed a model with a motion conversion network as the backbone [19]. The transformation network is designed in an encoder-decoder manner, which focuses on local motion while ignoring static regions. In order to focus on key objects, they further inserted an attention module before the conversion network, which has the advantage that more subtle motion information can be learned, but the computational cost will increase exponentially. Wu et al. proposed a two-stage method to separate dynamic objects from static backgrounds [20]—first training an object detection network to classify moving objects and static backgrounds, then predict future frames of static scenes, and then predict the motion of dynamic objects. Finally, the background is filled by the method of image filling to obtain the predicted frame. The reported results are quite accurate, but because of the additional target detection step, it needs to consume more resources, including computational overhead and manual labeling.

Generative adversarial networks have shown superior performance in image generation. The first video prediction method trained in an adversarial style was proposed by Mathieu et al. [21]. They designed a novel image gradient-based GDL regularization loss to replace the mean square error MSE to generate sharp video frames. Lee et al. proposed a typical stochastic adversarial video prediction method [22]. To address the problem of deterministic models averaging the future into a single, ambiguous prediction, the authors proposed using variational network to model the underlying randomness, and combined with adversarial training to generate clear visualizations. The reported predicted image quality

is good, but it underperforms on quantitative evaluations such as SSIM and PSNR. Simulating the human intelligence system is another popular way. Inspired by the characteristics of the frequency band decomposition of the human visual system, Jin et al. proposed to incorporate wavelet analysis into the prediction network [23], and cooperate with adversarial training to sharpen the image. The specific operation is to decompose the input video frame into multiple frequency band inputs through discrete wavelet transform. The idea is similar to content and motion separation, except that they are separated from the perspective of frequency.

3D convolutions can effectively preserve local dynamics and model short-term features. But it suffers from poor flexibility (for example, the dimension are usually fixed and the number of input or output frames cannot be adjusted casually), difficult training and long-distance video reasoning. Therefore, some people attempt to combine 3D convolution and recurrent neural network to improve the flexibility of learning and reasoning while preserving short-term features. E3D-LSTM is a typical 3D video prediction model proposed by Wang et al. [17]. They divide the input video sequence into several groups, and each group contains  $T$  video frames. Then, they use 3D convolutions for video group encoding, which are fed into LSTM nested with 3D convolutions for prediction. The 3D convolution is responsible for learning the short-term memory within each group, and the LSTM performs long-term modeling to effectively manage long-term historical memory. The disadvantage is that the training is difficult and the calculation overhead is large—every time a video frame is predicted, a set of video sequences with a length of  $T$  needs to be input and calculated. Li et al. [24] used a 3D convolutional-based variational auto-encoder to model uncertainty, and their predictions were divided into two stages: first, the optical flow was predicted using a 3D variational auto-encoder, which describes pixel spatial layout. The predicted optical flow is then converted into predicted frames using the Flow2rgb model. Such a design avoids the model directly viewing the high-dimensional pixel space of video sequences.

The ability to predict and reason about future events is the essence of intelligence. Actually, early works on video prediction were inspired by the predictive coding paradigm [25], [26]. One of the most famous work on video prediction based on predictive coding is the PredNet model proposed by Lotter et al. [27]. It uses vertically stacked convolutional LSTM (ConvLSTM) [28] as the main carrier, and strictly follows the computing style of the traditional predictive coding framework: lower-level neurons transmit prediction errors upward, and higher-level neurons propagate predictions downward. The presented results are superior to the contemporaneous work [21], but they only explored the prediction results of the next frame and did not report the performance on long-term prediction. Similarly, Elsayed et al. [29] also used ConvLSTM to construct a predictive coding based video prediction model. In order to reduce the computational overhead, they tried to reduce the model parameters and training time by reducing the gating calculation in LSTM, but they also only reported the prediction results of the next frame. Straka et

al. constructed a video prediction model named PrecNet by imitating the PredNet model [30]. They changed the direction of the information flow—propagating prediction upward and prediction error downward, which is the opposite of how predictive coding is computed, but the authors did not report the reason.

In summary, there are still some problems in the existing video prediction models or methods: First, there is still room for improvement in the architecture of the network. For example, the Encoder-LSTM-Decoder network only performs predictions in the high-level semantic space, ignoring most of the low-level details. Secondly, the calculation cost is too large (such as E3D-LSTM), which consumes a lot of resources and is not conducive to the final application. Finally, the problem of training-testing mismatch during long-term prediction is not well addressed.

### III. METHODS

In this paper, we make two major improvements to address the above problems. First, we combine the predictive coding theory and the coarse-to-fine approach to design a multi-scale predictive coding model (MSPN). The model is updated and corrected by the combination of top-down and bottom-up information flows, where the neurons of local network level predict an RGB image of the future frame at a lower resolution. On the one hand, the predicted frame will be propagated down to gradually restore the pixels. On the other hand, it will be compared with the next input frame to compute the prediction errors. The errors carry information about the mismatch between predictions and actual sensory inputs, to correct and update the internal representation of local neurons. At the same time, it will be propagated upwards to guide the update of higher-level neurons, thus forming effective feedback connections. Particularly, we use LSTM integrated with an encoder-decoder network to encode the pixel-level inputs and generate predicted images. The hidden state of LSTM is fixed to a small depth in each network level, only the necessary information is retained and updated. It can avoid being mapped to a more discrete and complex space in this way, thus reducing computational overhead and the difficulty of prediction. Furthermore, To enhance the connection between different network levels, we share the highest-level semantic information encoded by the encoder in different levels.

In addition, we also explore the training strategies. We use adversarial training to sharpen the generated images. However, adversarial training is unstable. Intuitively, the generation of images is much more difficult than its discrimination, so there is often the case that the discriminator converges while the generator diverges during training. To alleviate this problem, we propose an iterative control method—when the discriminator judges that the score of the real frame exceeds a threshold than the predicted frame, we fix the discriminator and train the generator until their scores are similar. This ensures that the discriminator is always slightly stronger than the generator, avoiding vanishing gradients or learning wrong gradients by the generator. In addition, in order to achieve continuous prediction, it is necessary to

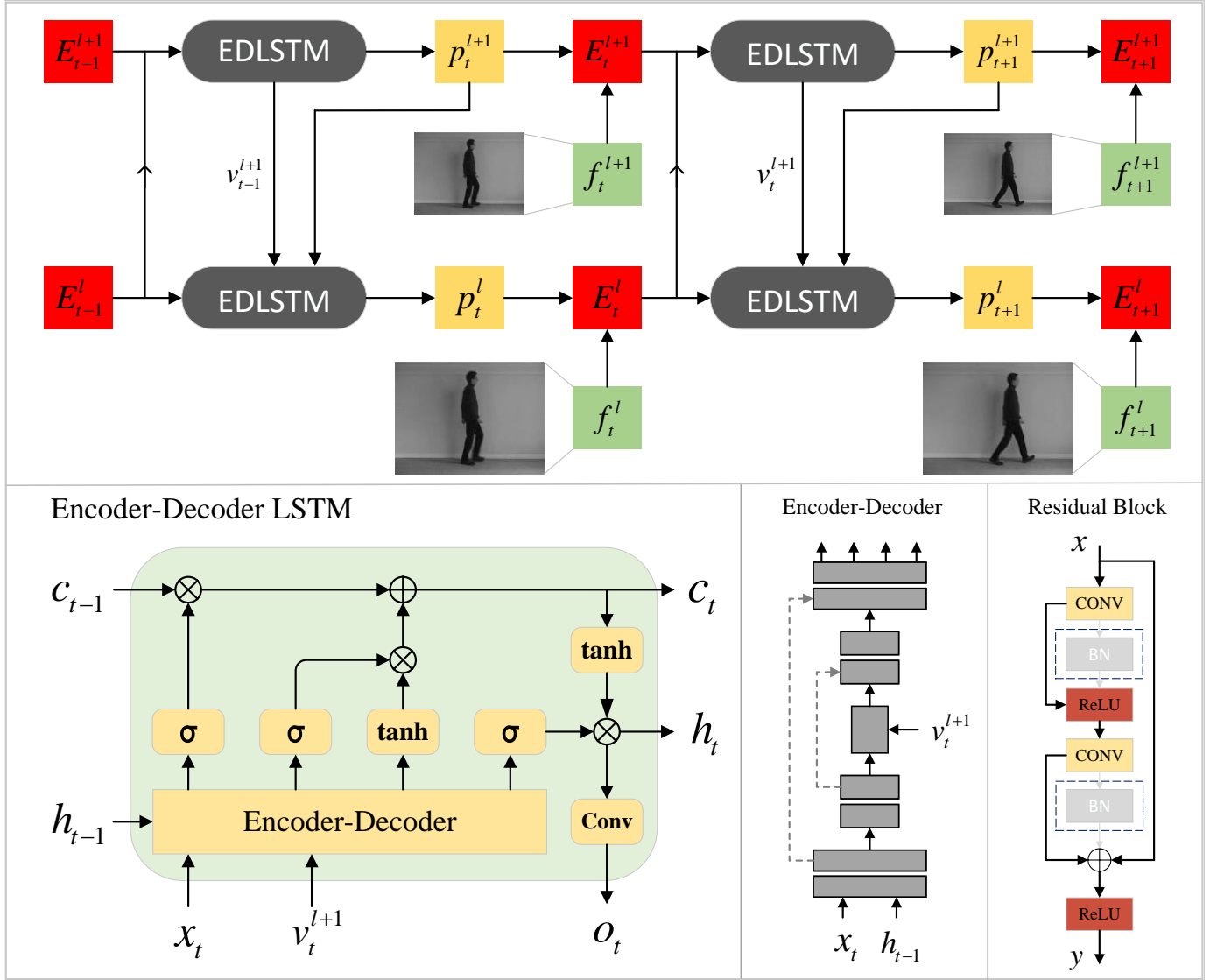


Fig. 2. The overview of multi-scale predictive network architecture, where  $P_t^l$ ,  $E_t^l$ ,  $f_t^l$  denote the predicted RGB image, prediction error and the input frame at time-step  $t$  and level  $l$ , respectively. At the bottom, the figure shows the detailed structure of encoder-decoder LSTM module, where  $v_t^{l+1}$  represents the encoded high-level semantic information from higher level,  $o_t$  denotes the output RGB image. The definition of other parameters is the same as the regular LSTM network.

use the predicted frame as a new input, thus resulting in the problem of mismatch between training and testing. The predicted frame may be blurry or incorrect, which will lead to the accumulation of prediction errors, which will eventually lead to increasingly blurred generated images. Therefore, we propose to use predicted frames as input during training, allowing the model to learn how to use predicted frames to generate more reliable future frames. More details will be introduced in the following subsections.

#### A. Network Model

**Network Architecture** The overall architecture of multi-scale predictive network is shown in Fig 2, which uses Encoder-Decoder LSTM (EDLSTM) as the main carrier and follows a strict top-down and bottom-up propagation manner of information flow. In the figure,  $f_t^l$  denotes the RGB image

at time-step  $t$  and level  $l$ , which is obtained by directly downsampling the original input frame. In the actual calculation, we obtain the RGB image of each level through  $2 \times$  downsampling, whose size can be defined as  $(B, 3, \frac{H}{2^l}, \frac{W}{2^l})$ , where  $B$ ,  $H$  and  $W$  denote batch-size, high and width of the original input, respectively. The  $P_t^l$  denotes prediction made by neurons at level  $l$  and time-step  $t$ , its purpose is to predict the RGB image  $f_t^l$ . By computing the difference between the prediction  $P_t^l$  and RGB image  $f_t^l$ , we can obtain the prediction error  $E_t^l$ . It is defined as the collective of positive and negative errors  $E_t^l = C[|f_t^l - P_t^l|, |P_t^l - f_t^l|]$ , where  $C$  represents concatenating two tensors together by channel  $(B, 6, \frac{H}{2^l}, \frac{W}{2^l})$ . This design has its biological basis—there are two populations of error computing neurons, one of which is dedicated to positive errors and the other to negative errors [1]. The prediction error is used to update and correct the internal representation of neurons. When the scene is predictable, its signal is sparse, so

the predictive coding model is efficient.

In general, the EDLSTM units in each level receive three kinds of inputs: predictions from higher level  $P_t^{l+1}$  (except the highest level), prediction errors from the local level  $E_{t-1}^l$  and lower level  $E_{t-1}^{l-1}$  (except the lowest level), to make local prediction  $P_t^l$ . Since the input signal is at the pixel level, it is necessary to use a codec network to realize the encoding and decoding of information. Different from the traditional Encoder-LSTM-Decoder model, we directly encapsulate an Encoder-Decoder network which is connected in a skip-connection manner into the LSTM network (Fig 2) to enhance the predictive ability. In the actual calculation, it first concatenates the current input signal  $x_t$  and previous hidden state  $h_{t-1}$ , and then uses the codec network for end-to-end calculation. Next, we split the output of the encoder-decoder network into 4 kinds of gating signals, followed by LSTM gating calculation. Finally, the output RGB image is obtained by performing another convolutional calculation on the current hidden state  $h_t$ .

Since the final output of each level is a 3-channel RGB image, the hidden state of LSTM only needs to retain and update the necessary information that can be restored into an RGB image. As a result, it can be fixed to a smaller depth (we set it to 64-channel in this work) to avoid being mapped to a more discrete and complex space as the level increases, thus reducing the difficulty of prediction and computational overhead. In addition, it is insufficient to connect between different network levels only by pixel-level signals. In order to enhance the connection, we share the high-level semantic information encoded by higher-level neurons. As shown in Fig 3, we propagate down the encoded hidden variable  $v_t^{l+1}$  obtained by the higher-level encoder network, which will be combined with the output of local encoder  $v_t^l$  to update and calculate a new hidden variable (Eq. 1, where  $f(\cdot)$  represents convolutional calculation and  $\theta$  denotes the parameters).

$$v_t^l \leftarrow f(v_t^l, v_t^{l+1}, \theta) \quad (1)$$

Importantly, we use a series of residual blocks with normalization layers removed as the base modules for encoder-decoder network. Though normalization has played an active role in tasks such as image classification, we proposed that in the tasks of image-to-image generation, it is not conducive to the convergence of training. Normalization is first proposed to solve the problem of internal covariate shift [31]. It will reduce the absolute difference between images and highlight the relative difference, to speed up training. Besides, it pays more attention to the texture of the image than the shape, so it performs well on coarse-grained tasks such as image classification. However, in the fine-grained tasks of image-to-image generation, the absolute difference and the shape of images is especially important [32]. In the work of StyleGAN2 [33], Karras et al. also make improvements on the quality of generated images by removing the normalization layers. Actually, tasks such as video prediction are designed to learn differences in image sequences, so it is better to remove the normalization layers.

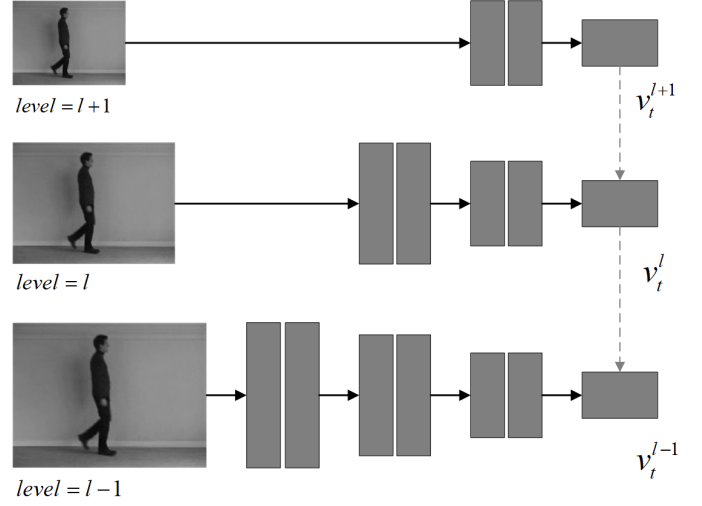


Fig. 3. We share the high-level semantic information encoded by higher-level neurons. The  $v_t^l$  denotes the final encoded features at time-step  $t$  and level  $l$ . We reduce the number of network layers in higher-level, to ensure that the input of each level is encoded into features of the same size (different depth (channels), and the depth of higher level is smaller) while reducing computational overhead. Then the higher-level encoded features  $v_t^{l+1}$  are passed down, and the lower-level encoded features  $v_t^l$  are calculated and updated.

**Algorithm** The calculation of multi-scale predictive model is described in Algorithm 1, which is implemented by calculating the bidirectional information flow—we first initialize the prediction errors at each level to zero. In the top-down information flow computation (line 4-11 in Algorithm 1), higher-level EDLSTM units receive the prediction error of previous time-step  $E_{t-1}^l$ , the prediction  $p_t^{l+1}$  from higher level (except the highest level) and the prediction error  $E_{t-1}^{l-1}$  from lower level (except the lowest level) to make local prediction  $P_t^l$ , and then propagate down the prediction  $P_t^l$  and the encoded latent variable  $v_t^l$ . Next, in the bottom-up computational flow (line 13-16 in Algorithm 1), we calculate

---

**Algorithm 1** Calculation of multi-scale predictive network

---

- 1: **Required:** video frames  $f_0, f_1, \dots, f_n$
  - 2: **Output:** predictive frames  $P_0, P_1, \dots, P_n$
  - 3: **for**  $t = 0$  to  $T$  **do**
  - 4:   **for**  $l = L$  to  $0$  **do**
  - 5:     **if**  $l == L$  **then**
  - 6:        $P_t^l, v_t^l = EDLSTM(E_{t-1}^l, E_{t-1}^{l-1})$
  - 7:     **else if**  $l == 0$  **then**
  - 8:        $P_t^l, v_t^l = EDLSTM(E_{t-1}^l, P_t^{l+1}, v_t^{l+1})$
  - 9:     **else**
  - 10:        $P_t^l, v_t^l = EDLSTM(E_{t-1}^l, E_{t-1}^{l-1}, P_t^{l+1}, v_t^{l+1})$
  - 11:     **end if**
  - 12:   **end for**
  - 13:   **for**  $l = 0$  to  $L$  **do**
  - 14:      $f_t^l = Downsample(f_t, size = (\frac{h}{2^l}, \frac{w}{2^l}))$
  - 15:      $E_t^l = [ReLU(f_t^l - p_t^l), ReLU(p_t^l - f_t^l)]$
  - 16:   **end for**
  - 17: **end for**
-

the prediction targets  $f_t^l$  for higher levels by downsampling the input frame, followed by calculating the difference between targets and predictions and updating the prediction error  $E_t^l$ .

### B. Training strategies

**Training Loss** We directly use the Euclidean distance instead of the mean squared error as the loss function. The mean square error is divided by the total number of pixels on the basis of square error, which can easily cause the gradient to be too small or even disappear, and eventually lead to blurring of the generated image. The computation is defined as Eq. 2:

$$\mathcal{L}_{pix} = \sum_{t=0}^T \sum_{l=0}^L \lambda_t \lambda_l \| Y_t^l - \hat{Y}_t^l \|^2 \quad (2)$$

where  $Y_t^l$  and  $\hat{Y}_t^l$  denote the ground truth frame and predicted RGB image respectively at level  $l$  and time-step  $t$ .  $\lambda_t$  and  $\lambda_l$  are the weighting factors by time and network level.

In order to solve the ambiguity caused by the deterministic loss function, the adversarial training is also introduced to sharpen the predicted frame. We try to build a discriminator which also uses residual block as the main carrier to guide the predictive model to generate more realistic frames. The adversarial losses are defined as follows:

$$\mathcal{L}_D = \mathbb{E}_{x \sim p(x)}[D(x)] + \mathbb{E}_{z \sim p(z)}[1 - D(G(z))] \quad (3)$$

$$\mathcal{L}_G = \mathbb{E}_{z \sim p(z)}[D(G(z))] \quad (4)$$

where  $G$  and  $D$  denote the generator and discriminator respectively. The discriminator tries to seek out the difference between the generated frame  $G(z)$  ( $z$  denotes the input signals of generator) and the real frame  $x$  to make distinction. When training the discriminator, we maximize the expectations  $D(x)$  and  $1 - D(G(z))$  to make the discriminator distinguish between real frames and predicted frames as much as possible. On the contrary, we maximize the expectation  $D(G(z))$  while training the generator. In particular, we abandon the cross-entropy classification method but directly score the input images, to better guide the learning of generator. The total loss of generator is designed as the combination of pixel loss and adversarial loss:

$$\mathcal{L}_{total} = \mathcal{L}_{pix} + \lambda \mathcal{L}_G \quad (5)$$

where  $\lambda$  denotes the weighting factor. Compared with the adversarial loss, pixel loss is easier to guide the learning of the network and limit its optimization direction, so that the generator will not generate realistic but incorrect frames. However, this limitation may still cause the final generated image to be blurry, so we need a larger value for  $\lambda$ .

**Improved Adversarial Training** It is already a consensus that adversarial training is difficult. Intuitively, the generation of an image is much more difficult than its discrimination. So there is often a problem that the discriminator is over-trained, which leads to the disappearance of learning

---

### Algorithm 2 Improved adversarial training manner

---

```

1: Required: input signal  $z_0, z_1, \dots, z_n$ , real video frames
    $f_0, f_1, \dots, f_n$ , weighting factor  $\lambda$ , tolerance  $c_1, c_2$ 
2: for  $epoch = 0$  to  $m$  do
3:   / Train discriminator /
4:   while  $True$  do
5:      $P_n = G(z_n)$ 
6:      $P_s, R_s = D(P_n), D(f_n)$ 
7:      $\mathcal{L}_D = (R_s - 1)^2 + (P_s + 1)^2$ 
8:     backward  $\mathcal{L}_D$ 
9:     if  $P_s < R_s - c_1$  then
10:      Break
11:    end if
12:  end while
13:  / Train generator /
14:  while  $True$  do
15:     $P_n = G(z_n)$ 
16:     $P_s, R_s = D(P_n), D(f_n)$ 
17:     $\mathcal{L}_G = (P_s - 1)^2$ 
18:     $\mathcal{L}_{total} = \mathcal{L}_{pix} + \lambda \mathcal{L}_G$ 
19:    backward  $\mathcal{L}_{total}$ 
20:    if  $P_s > R_s - c_2$  then
21:      Break
22:    end if
23:  end while
24: end for

```

---

gradient. In this work, we try to alleviate such a problem by first training the discriminator to preliminarily distinguish between real frames and predicted frames, that is, the score of real frames is higher than that of predicted frames. However, when the score of real frame is much higher than that of the predicted frame, the discriminator is fixed and the generator is trained until the score of predicted image is close to but still smaller than the real frame. At this point, the generator is fixed and the discriminator is trained, and so on. In this way, the discriminator is always slightly stronger than the generator, which prevents the discriminator from overtraining and the generator from learning the wrong gradients.

The total implementation of training is shown in Algorithm 2, where  $P_s, R_s$  denote scores of predictive frames and real frames respectively. Tolerance  $c_1$  and  $c_2$  are two constants where  $c_1$  is less than  $c_2$ . During training, the scores of the predicted frames are always kept within a fixed range ( $R_s - c_2 < P_s < R_s - c_1$ ), so that the discriminator is always slightly stronger than the generator, thus better guiding the learning of the generator.

**Long-term Prediction** The mismatch between training and testing is a problem that has not been solved fundamentally in image sequence prediction. The model is supported by the ground truth frames during training, while it is necessary to use the predicted frames as new input for continuous prediction during testing. There is a distance between the predicted frame and ground truth frame, thus resulting in mismatch between training and testing. Moreover, in the calculation of recurrent neural network based on the Markov chain,

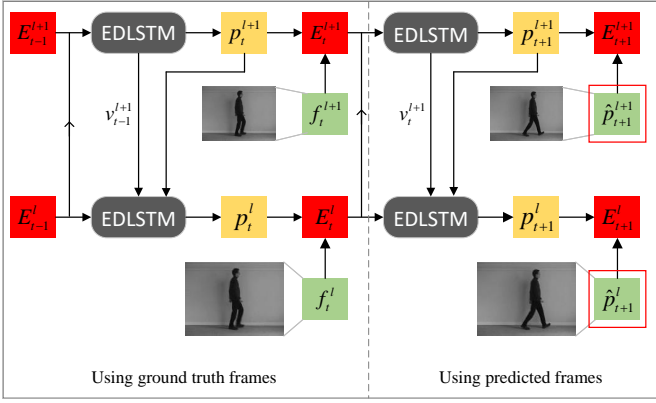


Fig. 4. The model is trained to learn to make prediction continuously by serving predicted frames as new inputs.  $\hat{P}_{t+1}^l$  denotes the RGB input image of level  $l$  downsampled from the original predicted frame  $P_{t+1}^0$ .

when a bad result is produced at a certain time step, it will inevitably affect the subsequent learning. Therefore, with the accumulation of prediction errors, the predicted frames will become increasingly blurry, which is more pronounced when using deterministic prediction methods, mainly manifested as motion blur, ghosting, etc. In order to alleviate such a problem, we propose to adjust the training strategies.

As shown in Fig 4, we directly use predicted frames as input during training, trying to train the model to learn to extract effective information from predicted frames and suppress the impact of prediction errors. We first use  $T$  consecutive ground truth video frames as input for calculation to obtain the next predicted future frame, which is then served as new input frame for the next step of calculation and prediction. Note that higher-level input frames  $\hat{P}_{T+1}^l$  are obtained by directly downsampling the predicted frame  $P_{T+1}$  instead of local prediction  $P_{T+1}^l$ . Specifically, at time step  $T + 1$ , the higher-level EDLSTM units utilize information such as prediction error and hidden state of previous time-step to generate predictions, which is then propagated down to gradually restore the original resolution, that is, the final output predicted frame  $P_{T+1}$ . Next, it is down-sampled (interval sampling or pooling) and propagated to higher levels to calculate and update the prediction errors for the next loop of computation.

#### IV. EXPERIMENTS

In this section, we will first introduce the details of the experimental setup, including the quantitative evaluation metrics used in the task of video prediction and the settings of hyperparameters. Next, we will compare with the state-of-the-art methods on the five commonly used datasets of Moving MNIST [34], KTH [35], Human3.6M [36], Caltech [37] and KITTI [38]. We try our best to preprocess the datasets as closely as existing methods [21], [27], [30], [39], and directly make comparison with the demonstrated results. Finally, we conduct an ablation study on the training strategy proposed in this paper and whether to use batch normalization to highlight the effectiveness of our proposed method.

#### A. Experimental Setup

**Quantitative Metrics** Structural Similarity Index Measure (SSIM) [40] and Peak Signal to Noise Ratio (PSNR) [41] are commonly used to evaluate the similarity between two images. The SSIM is calculated from three aspects of illumination, contrast and structure, which is defined as Eq. 6

$$SSIM(x, y) = \frac{(2\mu_x\mu_y + c_1)(2\sigma_{xy} + c_2)}{(\mu_x^2 + \mu_y^2 + c_1)(\sigma_x^2 + \sigma_y^2 + c_2)} \quad (6)$$

where  $\mu_x, \mu_y$  denote mean of  $x, y$  respectively, and  $\sigma$  indicate variance.  $c_1$  and  $c_2$  are two constants used to maintain stability to avoid division by zero. The PSNR is a metric for measuring the image quality between the maximum signal and background noise, which is defined as Eq. 7

$$PSNR = 10 \cdot \log_{10}\left(\frac{MAX_I^2}{MSE}\right) \quad (7)$$

where  $MSE$  denotes the *mean square error* and  $MAX_I^2$  indicates the possible maximum pixel value of the images. Besides, we also introduce a recent popular indicator called Learned Perceptual Image Patch Similarity (LPIPS) [42] to measure the difference between two images. It focuses on perceptual similarity rather than quality assessment, which is more in line with human perception compared to the traditional metrics. Higher scores of SSIM and PSNR, and lower scores of LPIPS indicate better results.

**Experimental Setting** We use PyTorch as platform and Adam [43] as optimizer to implement the algorithm described above. The length of input sequence is fixed at 10 for training and testing, and the number of network levels is set to 4. Other hyper-parameters and introductions are shown in Table I.

TABLE I  
SETTING OF HYPERPARAMETERS FOR TRAINING, WHERE  $\lambda_t, \lambda_l$  AND  $\lambda$  DENOTE THE WEIGHTING FACTORS DESCRIBED IN EQ. 2 AND EQ. 5. “ $L$ ” INDICATES THE NUMBER OF NETWORK LEVELS.

parameters	values	introductions
$lr_g$	$1 \times 10^{-3}$	learning rate of generator
$lr_d$	$10^{-7} \sim 10^{-9}$	learning rate of discriminator
$\lambda_t$	$0, t = 0$ $1, t > 0$	weighting factor by time
$\lambda_l$	$(L - l)/L$	weighting factor by level
$\lambda$	10	weighting factor of generator loss

#### B. Experimental results

**KTH** The KTH is one of the most commonly used datasets for task of video prediction. It is very popular due to its moderate complexity of scene and event (the dataset contains only 6 action categories on a simple backgrounds). Similar to previous works, we use person 1-16 for training and person 17-25 for testing, and use 10 frames as input to predict the next 10 and 30 frames. The quantitative evaluation results are shown in Table II. The results of previous works are excerpted from [23], [44] and [45]. As shown in the table, our method achieve comparable or better performance compared

TABLE II  
QUANTITATIVE EVALUATION ON THE KTH DATASET. THE METRICS ARE AVERAGED OVER THE PREDICTED FRAMES. RED AND BLUE INDICATE THE BEST AND SECOND BEST RESULTS, RESPECTIVELY.

Methods	10 $\rightarrow$ 20			10 $\rightarrow$ 40		
	SSIM $\uparrow$	PSNR $\uparrow$	LPIPS $\downarrow$	SSIM $\uparrow$	PSNR $\uparrow$	LPIPS $\downarrow$
MCNet [18]	0.804	25.95	-	0.73	23.89	-
fRNN [47]	0.771	26.12	-	0.678	23.77	-
PredRNN [48]	0.839	27.55	-	0.703	24.16	-
PredRNN++ [49]	0.865	28.47	-	0.741	25.21	-
VarNet [39]	0.843	28.48	-	0.739	25.37	-
SAVP-VAE [22]	0.852	27.77	8.36	0.811	26.18	11.33
E3D-LSTM [17]	0.879	29.31	-	0.810	27.24	-
STMF [23]	0.893	29.85	11.81	0.851	27.56	14.13
Conv-TT-LSTM [46]	0.907	28.36	13.34	0.882	26.11	19.12
LMC-Memory [44]	0.894	28.61	13.33	0.879	27.50	15.98
PPNet [45]	0.886	31.02	13.12	0.821	28.37	23.19
MSPN (ours)	0.881	31.87	7.98	0.831	28.86	14.04

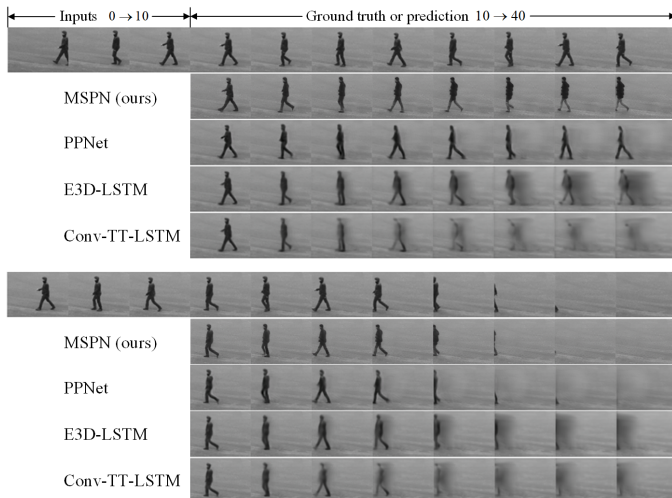


Fig. 5. Visualization examples on the KTH datasets. We use 10 frames as input to predict next 30 frames. The other results are obtained from [45]. Zoom in for a better view.

with the state-of-the-art methods. In addition, our model converges fast, which only takes about 20 epochs to achieve good performance. Figure 5 shows the visualization examples on the KTH dataset. As we can observe from the figure, our method can also achieve good visual results, while the Conv-TT-LSTM [46], which obtains the highest SSIM score, shows poor performance on the qualitative evaluation. The mismatch between quantitative and qualitative assessments remains an unsolved problem for video prediction tasks. We will discuss this issue in the conclusion section.

**Moving MNIST** The Moving MNIST is an early popular synthetic dataset for video representation learning. Its scenarios and events are very simple, each sequence is 20 in length and shows how 2 digits move at a constant speed and bounce within a  $64 \times 64$  box. Similarly, we use 10 frames as input to predict the next 10 frames. Table III shows the quantitative evaluation results on SSIM and MSE, the results of previous works are excerpted from [50] and [44]. Figure 6 shows the

TABLE III  
QUANTITATIVE EVALUATION ON THE MNIST DATASET. THE METRICS ARE AVERAGED OVER THE 10 PREDICTED FRAMES. RED AND BLUE INDICATE THE BEST AND SECOND BEST RESULTS, RESPECTIVELY.

Methods	10 $\rightarrow$ 20	
	SSIM $\uparrow$	MSE $\downarrow$
2D ConvLSTM [28]	0.763	82.2
PredRNN++ [49]	0.870	47.9
E3D-LSTM [17]	0.910	41.3
Variational 2D ConvLSTM [51]	0.816	60.7
Improved VRNN [52]	0.776	129.2
Variational 3D ConvLSTM [50]	0.896	39.4
Conv-TT-LSTM [46]	0.915	53.0
LMC-Memory [44]	0.924	41.5
MSPN (Ours)	0.926	39.5

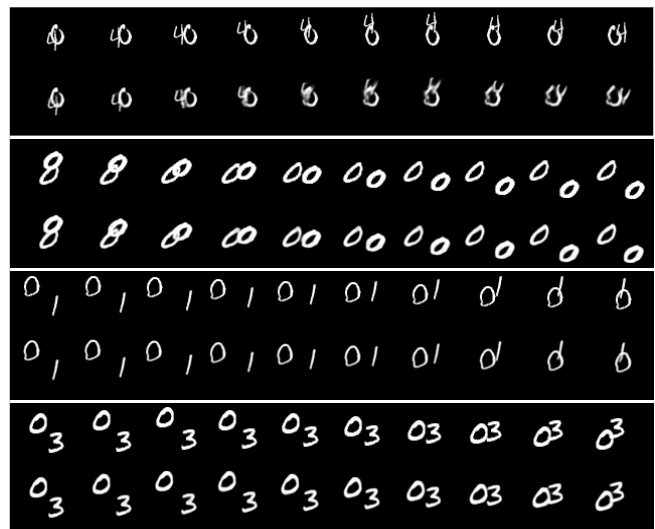


Fig. 6. Visualization examples on the MNIST datasets. We use 10 frames as input to predict next 10 frames. In each group, the first row indicates the ground truth frames and the second row indicates predicted frames. Zoom in for a better view.

visualization examples, we have tried our best to search the demonstrated examples of previous works, but unfortunately none have been found, so we only present our results in the figure. Since the scenes and events are simple, we did not use adversarial training to sharpen the generated images to save training overhead. Nevertheless, we can still achieve good performance from the perspective of qualitative evaluation. Actually, most of the background pixels in this dataset are zeros. If we set a threshold and change the predicted pixels smaller than the threshold to zeros, we will get higher accuracy ( $MSE = 37.1$ ). Therefore, we consider that the MNIST dataset may no longer be suitable for video prediction task in the future (anyone can improve the accuracy on this dataset with several deliberate modifications, but these modifications are not suitable for other scenarios).

**Human3.6M** Human3.6M is a large public dataset for 3D human pose estimation research. Due to the time series



TABLE IV  
QUANTITATIVE EVALUATION ON THE HUMAN3.6M DATASET. THE BEST RESULTS ARE MARKED IN BOLD, WHERE THE RESULTS OF OTHER WORKS ARE EXCERPTED FROM [53]

Methods	Metric	T=2	T=4	T=6	T=8	T=10
MCNet [18]	PSNR	30.0	26.55	24.94	23.90	22.83
	SSIM	0.9569	0.9355	0.9197	0.9030	0.8731
	LPIPS	0.0177	0.0284	0.0367	0.0462	0.0717
fRNN [47]	PSNR	27.58	26.10	25.06	24.26	23.66
	SSIM	0.9000	0.8885	0.8799	0.8729	0.8675
	LPIPS	0.0515	0.0530	0.0540	0.0539	0.0542
MAFENet [53]	PSNR	31.36	28.38	26.61	25.47	24.61
	SSIM	0.9663	0.9528	0.9414	0.9326	0.9235
	LPIPS	0.0151	<b>0.0219</b>	<b>0.0287</b>	<b>0.0339</b>	<b>0.0419</b>
MSPN(Ours)	PSNR	<b>31.95</b>	<b>29.19</b>	<b>27.46</b>	<b>26.44</b>	<b>25.52</b>
	SSIM	<b>0.9687</b>	<b>0.9577</b>	<b>0.9478</b>	<b>0.9382</b>	<b>0.9293</b>
	LPIPS	<b>0.0146</b>	0.0271	0.0384	0.0480	0.0571

characteristics of its original image data, it has also been used in video prediction tasks by many works. The dataset is obtained by collecting videos of performers’ actions in a designated room. Similar to the work [53], we use S11 for testing, the others for training, and the image is cropped and then adjusted to  $128 \times 128$  size. Table IV and Figure 7 show the quantitative evaluation and qualitative evaluation results on this dataset, respectively. Among them, the results of other works are excerpted from [53]. We couldn’t find a visualization example which is exactly the same as work [53], but could obtain the original data with a high similarity to this example, so Figure 7 shows the performance on this set of data. Although the accuracy reported in Table IV is high, the models seem to fail to restore the actions of the human very well. This is caused by the characteristics of this dataset—the static background occupies a large part of the image sequence, and the models only need to retain and restore these backgrounds to achieve a high accuracy. As a result, the models tend to learn and restore the static background in the sequence, while ignoring the actions of the human in the image.

**Caltech and KITTI** Caltech Pedestrian and KITTI are the other two popular datasets for video prediction task, which are obtained by collecting the traffic conditions, so the scenarios and events are more complex. Compared to Caltech, the KITTI dataset varies more between frames and is therefore harder to predict. Similarly, we resize the images to a resolution of  $128 \times 160$  for clear comparison and to reduce the computational overhead. Table V shows the quantitative evaluation results for the next 5 frames and 10 frames on these two datasets. Obviously, the performance on the KITTI dataset is much worse. Nevertheless, we still obtain better results than existing works. Figure 8 shows the visualization examples on the Caltech dataset. In contrast, the proposed method can recover more details. Since there are few results on the KITTI dataset, we failed to find any similar visualization examples on the original dataset, so the qualitative evaluation with other works will not be shown here.

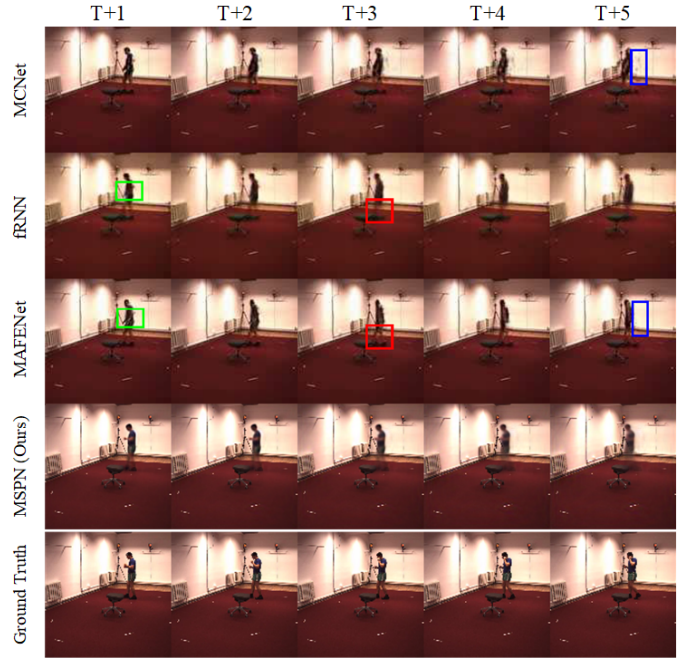


Fig. 7. Visualization examples on the Human3.6M dataset. We use 10 frames as input to predict the next frame. The other results are obtained from [54]. Zoom in for a better view.



Fig. 8. Visualization examples on the Caltech dataset. We use 10 frames as input to predict the next frame. The other results are obtained from [54]. Zoom in for a better view.

### C. Ablation study

**Different Training Strategies** We observed that the training strategies have a significant impact on the quality of predictions, especially the visualization of predicted frames. We conducted several comparative experiments on the KTH, Caltech and KITTI datasets to explore the impact of three different training strategies on the experimental results. Table VI and Figure 9 show the quantitative evaluation and quality evaluation results with different training strategies on the three datasets, respectively. Among them, “WO.T.” denotes “Without Training”, which represents the traditional training strategy that only the ground truth frames are used as input during training. “W.T.” denotes “With Training”, which

TABLE V  
 QUANTITATIVE EVALUATION ON THE CALTECH AND KITTI DATASET RESPECTIVELY. THE METRICS ARE AVERAGED OVER THE 0-5 AND 5-10 PREDICTED FRAMES. THE RESULTS OF RELATED WORKS ARE EXTRACTED AND COMPUTED FROM [20].

Methods	Caltech						KITTI					
	0-5			5-10			0-5			5-10		
	SSIM	PSNR	LPIPS	SSIM	PSNR	LPIPS	SSIM	PSNR	LPIPS	SSIM	PSNR	LPIPS
PredNet [27]	0.752	-	36.03	0.574	-	68.39	0.475	-	62.95	-	-	-
MCNET [18]	0.705	-	37.34	0.488	-	52.92	0.555	-	37.39	-	-	-
Voxel Flow [55]	0.711	-	28.79	0.557	-	44.31	0.426	-	41.59	-	-	-
Vid2vid [56]	0.751	-	20.14	0.587	-	33.96	-	-	-	-	-	-
FVSOMP [20]	0.756	-	16.50	0.592	-	30.06	0.608	-	<b>30.49</b>	-	-	-
MSPN (Ours)	<b>0.818</b>	23.88	<b>10.98</b>	<b>0.682</b>	19.87	<b>19.56</b>	<b>0.629</b>	19.44	32.10	0.447	15.69	46.52

TABLE VI  
 ABLATION STUDY ON THE KTH, CALTECH AND KITTI DATASET, RESPECTIVELY. THE METRICS ARE AVERAGED OVER THE 10 PREDICTED FRAMES. THE MEANINGS OF “Adv.,” “W.T.” AND “WO.T.” ARE DESCRIBED IN DETAIL IN THE TEXT.

Datasets	Methods	10 $\rightarrow$ 20		
		SSIM $\uparrow$	PSNR $\uparrow$	LPIPS $\downarrow$
KTH	Adv.	0.881	31.87	<b>7.98</b>
	W.T.	<b>0.896</b>	<b>32.43</b>	12.19
	WO.T.	0.892	32.33	13.26
Caltech	Adv.	0.750	21.88	15.27
	W.T.	<b>0.756</b>	<b>21.95</b>	<b>14.88</b>
	WO.T.	0.723	21.12	17.59
KITTI	Adv.	0.538	17.57	39.31
	W.T.	<b>0.552</b>	<b>17.99</b>	<b>38.19</b>
	WO.T.	0.495	15.77	40.01

indicates that the predicted frames are also used as input during training (described in Sec.3.B Long-term Prediction). “Adv.” denotes that the model is trained using the proposed adversarial training manner on the basis of “W.T.” training.

It can be observed that “W.T.” method is superior to “WO.T.” both in quantitative evaluation and qualitative evaluation. In particular, as the complexity of the scene and the inter-frame changes increase (such as Caltech and KITTI), the effect of “W.T.” is more significant—the more complex the scene, the more difficult it is to predict, so the faster the prediction error accumulates. As a result, the prediction accuracy of the conventional “WO.T.” training method drops sharply, while the “W.T.” method can better suppress the impact of prediction errors and achieve better performance. However, although the “W.T.” approach can slow down the degradation of prediction quality, it still suffers from the problem caused by training with deterministic loss—vagueness. Both Euclidean distance and mean square error tend to minimize the loss by averaging, which can easily blur the generated images. Therefore, we introduce the aforementioned adversarial training style to sharpen the generated images. Although the accuracy is somewhat worse than the “W.T.” method, it seems to generate better predictions from the perspective of human perception evaluation.

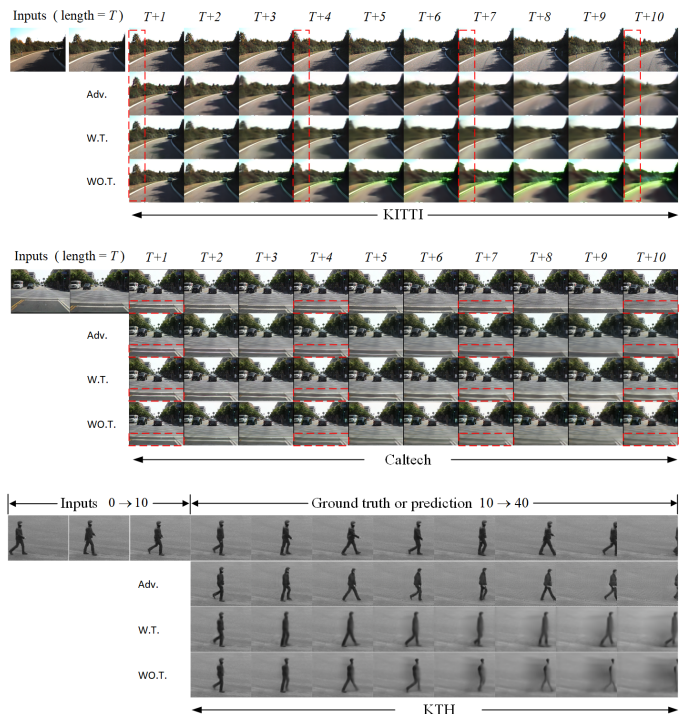


Fig. 9. Visualization examples on the KTH, Caltech and KITTI datasets, respectively. We use 10 frames as input to predict the next 10 frames (Caltech and KITTI) or 30 frames (KTH). The meanings of “Adv.,” “W.T.” and “WO.T.” are described in detail in the text. Zoom in for a better view.

**With or Without Batch Normalization** We have indicated that the Batch Normalization is not conducive to the convergence of training in task of image generation in Section 3.A. Several comparative experiments are conducted to verify this idea. We performed two sets of experiments on the KTH dataset with the batch size set to 8 and 16, respectively. We counted the prediction accuracy of the next frame within 30 epochs, and the results are shown in Figure 10. Obviously, training with BatchNorm layer removed is more stable, which converges faster, and works better. In addition, more memory and computational overhead can be reduced since there is no need to keep additional intermediate variables.

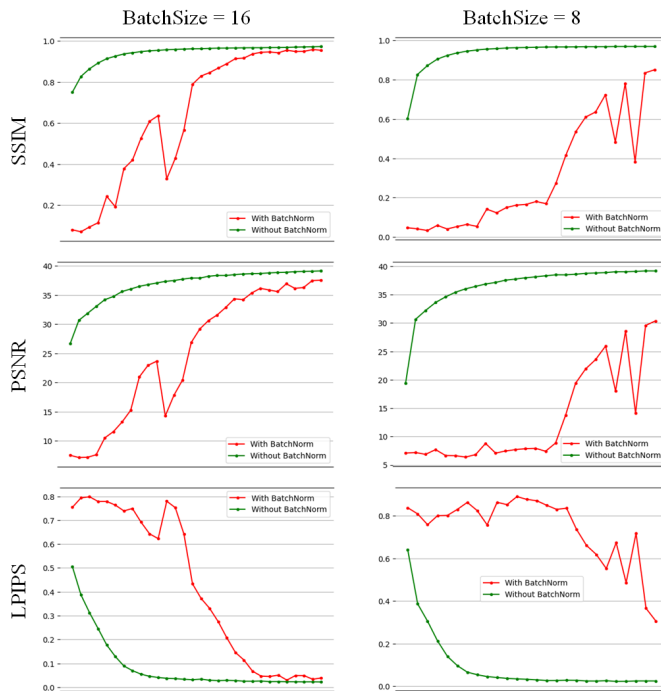


Fig. 10. We performed two sets of experiments on the KTH dataset with the batch size set to 8 and 16, respectively. The result is obtained by counting the prediction accuracy of the next frame within 30 epochs.

## V. CONCLUSION

In this paper, we combined the predictive coding theory, coarse-to-fine approach and deep learning architecture to design a multi-scale predictive model for the task of video prediction. We have analyzed the superiority of predictive coding model and pointed out the reason of designing the multi-scale predictive network. In addition, aiming at the problems which often occur in adversarial training, we proposed a novel training method which can prevent the discriminator from over-fitting and the generator from learning the wrong gradient. Furthermore, we also explored the influence of different training methods on the long-term prediction. We showed that the training methods have great influence on the final predictive results when the model and loss function are fixed. Importantly, we did get great performance on the task of video prediction with our methods. Nevertheless, the performance of our model and methods show powerless in complex scenarios. There is still huge room for improvement, we will further explore better methods to make predictions with higher accuracy and clarity in more complex scenarios.

## VI. ACKNOWLEDGMENT

This work was supported in part by the Key-Area Research and Development Program of Guangdong Province under Grant: 2019B090912001, and in part by the PolyU Start-up Grant: ZVUY-P0035417. The authors would like to thank the reviewing from editors and reviewers.

## REFERENCES

- [1] R. P. Rao and D. H. Ballard, "Predictive coding in the visual cortex: a functional interpretation of some extra-classical receptive-field effects," *Nature neuroscience*, vol. 2, no. 1, pp. 79–87, 1999.
- [2] B. Han and R. VanRullen, "The rhythms of predictive coding? prestimulus phase modulates the influence of shape perception on luminance judgments," *Scientific reports*, vol. 7, no. 1, pp. 1–10, 2017.
- [3] L. Aitchison and M. Lengyel, "With or without you: predictive coding and bayesian inference in the brain," *Current opinion in neurobiology*, vol. 46, pp. 219–227, 2017.
- [4] C. Teufel and P. C. Fletcher, "Forms of prediction in the nervous system," *Nature Reviews Neuroscience*, vol. 21, no. 4, pp. 231–242, 2020.
- [5] B. Wu, S. Nair, R. Martin-Martin, L. Fei-Fei, and C. Finn, "Greedy hierarchical variational autoencoders for large-scale video prediction," in *Proceedings of the IEEE/CVF Conference on Computer Vision and Pattern Recognition*, 2021, pp. 2318–2328.
- [6] H. Wu, Z. Yao, J. Wang, and M. Long, "Motionrnn: A flexible model for video prediction with spactime-varying motions," in *Proceedings of the IEEE/CVF Conference on Computer Vision and Pattern Recognition*, 2021, pp. 15 435–15 444.
- [7] B. Liu, Y. Chen, S. Liu, and H.-S. Kim, "Deep learning in latent space for video prediction and compression," in *Proceedings of the IEEE/CVF conference on computer vision and pattern recognition*, 2021, pp. 701–710.
- [8] Z. Chang, X. Zhang, S. Wang, S. Ma, and W. Gao, "Strpm: A spatiotemporal residual predictive model for high-resolution video prediction," in *Proceedings of the IEEE/CVF Conference on Computer Vision and Pattern Recognition*, 2022, pp. 13 946–13 955.
- [9] B. T. Morris and M. M. Trivedi, "Learning, modeling, and classification of vehicle track patterns from live video," *IEEE Transactions on Intelligent Transportation Systems*, vol. 9, no. 3, pp. 425–437, 2008.
- [10] A. Hu, F. Cotter, N. Mohan, C. Gurau, and A. Kendall, "Probabilistic future prediction for video scene understanding," in *European Conference on Computer Vision*. Springer, 2020, pp. 767–785.
- [11] C. Finn and S. Levine, "Deep visual foresight for planning robot motion," in *2017 IEEE International Conference on Robotics and Automation (ICRA)*. IEEE, 2017, pp. 2786–2793.
- [12] X. Shi, Z. Gao, L. Lausen, H. Wang, D.-Y. Yeung, W.-k. Wong, and W.-c. Woo, "Deep learning for precipitation nowcasting: A benchmark and a new model," *Advances in neural information processing systems*, vol. 30, 2017.
- [13] A. Bhattacharyya, M. Fritz, and B. Schiele, "Long-term on-board prediction of people in traffic scenes under uncertainty," in *Proceedings of the IEEE Conference on Computer Vision and Pattern Recognition*, 2018, pp. 4194–4202.
- [14] K. M. Kitani, B. D. Ziebart, J. A. Bagnell, and M. Hebert, "Activity forecasting," in *European Conference on Computer Vision*. Springer, 2012, pp. 201–214.
- [15] T. Han, W. Xie, and A. Zisserman, "Video representation learning by dense predictive coding," in *Proceedings of the IEEE/CVF International Conference on Computer Vision Workshops*, 2019, pp. 0–0.
- [16] J. Wang, J. Jiao, and Y.-H. Liu, "Self-supervised video representation learning by pace prediction," in *European conference on computer vision*. Springer, 2020, pp. 504–521.
- [17] Y. Wang, L. Jiang, M.-H. Yang, L.-J. Li, M. Long, and L. Fei-Fei, "Eidetic 3d lstm: A model for video prediction and beyond," in *International conference on learning representations*, 2018.
- [18] R. Villegas, J. Yang, S. Hong, X. Lin, and H. Lee, "Decomposing motion and content for natural video sequence prediction," in *International Conference on Learning Representations*, 2017.
- [19] X. Chen and W. Wang, "Uni-and-bi-directional video prediction via learning object-centric transformation," *IEEE Transactions on Multimedia*, vol. 22, no. 6, pp. 1591–1604, 2019.
- [20] Y. Wu, R. Gao, J. Park, and Q. Chen, "Future video synthesis with object motion prediction," in *Proceedings of the IEEE/CVF Conference on Computer Vision and Pattern Recognition*, 2020, pp. 5539–5548.
- [21] M. Mathieu, C. Couprie, and Y. LeCun, "Deep multi-scale video prediction beyond mean square error," *International conference on learning representations*, 2016.
- [22] A. X. Lee, R. Zhang, F. Ebert, P. Abbeel, C. Finn, and S. Levine, "Stochastic adversarial video prediction," *arXiv preprint arXiv:1804.01523*, 2018.
- [23] B. Jin, Y. Hu, Q. Tang, J. Niu, Z. Shi, Y. Han, and X. Li, "Exploring spatial-temporal multi-frequency analysis for high-fidelity and temporal-consistency video prediction," in *Proceedings of the IEEE/CVF Conference on Computer Vision and Pattern Recognition*, 2020, pp. 4554–4563.

- [24] Y. Li, C. Fang, J. Yang, Z. Wang, X. Lu, and M.-H. Yang, "Flow-grounded spatial-temporal video prediction from still images," in *Proceedings of the European Conference on Computer Vision (ECCV)*, 2018, pp. 600–615.
- [25] W. R. Softky, "Unsupervised pixel-prediction," in *Advances in neural information processing systems*, 1996, pp. 809–815.
- [26] A. Hollingworth, "Constructing visual representations of natural scenes: the roles of short-and long-term visual memory." *Journal of Experimental Psychology: Human Perception and Performance*, vol. 30, no. 3, p. 519, 2004.
- [27] W. Lotter, G. Kreiman, and D. Cox, "Deep predictive coding networks for video prediction and unsupervised learning," *International Conference on Learning Representations*, 2017.
- [28] X. Shi, Z. Chen, H. Wang, D.-Y. Yeung, W.-K. Wong, and W.-c. Woo, "Convolutional lstm network: A machine learning approach for precipitation nowcasting," *Advances in neural information processing systems*, vol. 28, 2015.
- [29] N. Elsayed, A. S. Maida, and M. Bayoumi, "Reduced-gate convolutional lstm architecture for next-frame video prediction using predictive coding," in *2019 International Joint Conference on Neural Networks (IJCNN)*. IEEE, 2019, pp. 1–9.
- [30] Z. Straka, T. Svoboda, and M. Hoffmann, "Precnet: Next frame video prediction based on predictive coding," *arXiv preprint arXiv:2004.14878*, 2020.
- [31] S. Ioffe and C. Szegedy, "Batch normalization: Accelerating deep network training by reducing internal covariate shift," in *International conference on machine learning*. PMLR, 2015, pp. 448–456.
- [32] B. Lim, S. Son, H. Kim, S. Nah, and K. Mu Lee, "Enhanced deep residual networks for single image super-resolution," in *Proceedings of the IEEE conference on computer vision and pattern recognition workshops*, 2017, pp. 136–144.
- [33] T. Karras, S. Laine, M. Aittala, J. Hellsten, J. Lehtinen, and T. Aila, "Analyzing and improving the image quality of stylegan," in *Proceedings of the IEEE/CVF conference on computer vision and pattern recognition*, 2020, pp. 8110–8119.
- [34] N. Srivastava, E. Mansimov, and R. Salakhudinov, "Unsupervised learning of video representations using lstms," in *International conference on machine learning*. PMLR, 2015, pp. 843–852.
- [35] C. Schuld, I. Laptev, and B. Caputo, "Recognizing human actions: a local svm approach," in *Proceedings of the 17th International Conference on Pattern Recognition, 2004. ICPR 2004.*, vol. 3. IEEE, 2004, pp. 32–36.
- [36] C. Ionescu, D. Papava, V. Olaru, and C. Sminchisescu, "Human3.6m: Large scale datasets and predictive methods for 3d human sensing in natural environments," *IEEE transactions on pattern analysis and machine intelligence*, vol. 36, no. 7, pp. 1325–1339, 2013.
- [37] P. Dollár, C. Wojek, B. Schiele, and P. Perona, "Pedestrian detection: An evaluation of the state of the art," *PAMI*, vol. 34, 2012.
- [38] A. Geiger, P. Lenz, C. Stiller, and R. Urtasun, "Vision meets robotics: The kitti dataset," *International Journal of Robotics Research (IJRR)*, 2013.
- [39] B. Jin, Y. Hu, Y. Zeng, Q. Tang, S. Liu, and J. Ye, "Varnet: Exploring variations for unsupervised video prediction," in *2018 IEEE/RSJ International Conference on Intelligent Robots and Systems (IROS)*. IEEE, 2018, pp. 5801–5806.
- [40] Z. Wang, A. C. Bovik, H. R. Sheikh, and E. P. Simoncelli, "Image quality assessment: from error visibility to structural similarity," *IEEE transactions on image processing*, vol. 13, no. 4, pp. 600–612, 2004.
- [41] A. Hore and D. Ziou, "Image quality metrics: Psnr vs. ssim," in *2010 20th international conference on pattern recognition*. IEEE, 2010, pp. 2366–2369.
- [42] R. Zhang, P. Isola, A. A. Efros, E. Shechtman, and O. Wang, "The unreasonable effectiveness of deep features as a perceptual metric," in *Proceedings of the IEEE conference on computer vision and pattern recognition*, 2018, pp. 586–595.
- [43] D. P. Kingma and J. Ba, "Adam: A method for stochastic optimization," *International conference on learning representations*, 12 2014.
- [44] S. Lee, H. G. Kim, D. H. Choi, H.-I. Kim, and Y. M. Ro, "Video prediction recalling long-term motion context via memory alignment learning," in *Proceedings of the IEEE/CVF Conference on Computer Vision and Pattern Recognition*, 2021, pp. 3054–3063.
- [45] C. Ling, J. Zhong, and W. Li, "Pyramidal predictive network: A model for visual-frame prediction based on predictive coding theory," *Electronics*, vol. 11, no. 18, p. 2969, 2022.
- [46] J. Su, W. Byeon, J. Kossaiif, F. Huang, J. Kautz, and A. Anandkumar, "Convolutional tensor-train lstm for spatio-temporal learning," *Advances in Neural Information Processing Systems*, vol. 33, pp. 13 714–13 726, 2020.
- [47] M. Oliu, J. Selva, and S. Escalera, "Folded recurrent neural networks for future video prediction," in *Proceedings of the European Conference on Computer Vision (ECCV)*, 2018, pp. 716–731.
- [48] Y. Wang, M. Long, J. Wang, Z. Gao, and P. S. Yu, "Predrnn: Recurrent neural networks for predictive learning using spatiotemporal lstms," *Advances in neural information processing systems*, vol. 30, 2017.
- [49] Y. Wang, Z. Gao, M. Long, J. Wang, and S. Y. Philip, "Predrnn++: Towards a resolution of the deep-in-time dilemma in spatiotemporal predictive learning," in *International Conference on Machine Learning*. PMLR, 2018, pp. 5123–5132.
- [50] H. Razali and B. Fernando, "A log-likelihood regularized kl divergence for video prediction with a 3d convolutional variational recurrent network," in *WACV (Workshops)*, 2021, pp. 209–217.
- [51] J. Chung, K. Kastner, L. Dinh, K. Goel, A. C. Courville, and Y. Bengio, "A recurrent latent variable model for sequential data," *Advances in neural information processing systems*, vol. 28, 2015.
- [52] L. Castrejon, N. Ballas, and A. Courville, "Improved conditional vrns for video prediction," in *Proceedings of the IEEE/CVF International Conference on Computer Vision*, 2019, pp. 7608–7617.
- [53] X. Lin, Q. Zou, X. Xu, Y. Huang, and Y. Tian, "Motion-aware feature enhancement network for video prediction," *IEEE Transactions on Circuits and Systems for Video Technology*, vol. 31, no. 2, pp. 688–700, 2020.
- [54] W. Yu, Y. Lu, S. Easterbrook, and S. Fidler, "Efficient and information-preserving future frame prediction and beyond," 2020.
- [55] Z. Liu, R. A. Yeh, X. Tang, Y. Liu, and A. Agarwala, "Video frame synthesis using deep voxel flow," in *Proceedings of the IEEE International Conference on Computer Vision*, 2017, pp. 4463–4471.
- [56] T.-C. Wang, M.-Y. Liu, J.-Y. Zhu, G. Liu, A. Tao, J. Kautz, and B. Catanzaro, "Video-to-video synthesis," *Conference on Neural Information Processing Systems (NeurIPS)*, 2018.